Geo-Marine Letters (2018) 38:227–240
https://doi.org/10.1007/s00367-017-0530-6

ORIGINAL

The Seno Otway pockmark field and its relationship to thermogenic gas occurrence at the western margin of the Magallanes Basin (Chile)

R. Kilian[1,2] · S. Breuer[3] · J. H. Behrmann[4] · O. Baeza[1] · M. Diaz-Michelena[5] · E. Mutschke[2] · H. Arz[6] · F. Lamy[7]

Received: 23 November 2017 / Accepted: 5 December 2017 / Published online: 15 December 2017

Abstract

Pockmarks are variably sized crater-like structures that occur in young continental margin sediments. They are formed by gas eruptions and/or long-term release of fluid or gas. So far no pockmarks were known from the Pacific coast of South America between 51°S and 55°S. This article documents an extensive and previously unknown pockmark field in the Seno Otway (Otway Sound, 52°S) with multibeam bathymetry and parametric echosounding as well as sediment drill cores. Up to 31 pockmarks per square kilometer occur in water depths of 50 to >100 m in late glacial and Holocene sediments. They are up to 150 m wide and 10 m deep. Below and near the pockmarks, echosounder profiles image acoustic blanking as well as gas chimneys often crosscutting the 20 to >30 m thick glacial sediments above the acoustic basement, in particular along fault zones. Upward-migrating gas is trapped within the sediment strata, forming dome-like features. Two 5 m long piston cores from inside and outside a typical pockmark give no evidence for gas storage within the uppermost sediments. The inside core recovered poorly sorted glacial sediment, indicating reworking and re-deposition after several explosive events. The outside core documents an undisturbed stratigraphic sequence since ~15 ka. Many buried paleo-pockmarks occur directly below a prominent seismic reflector marking the mega-outflow event of the Seno Otway at 14.3 ka, lowering the proglacial lake level by about 80 m. This decompression would have led to frequent eruptions of gas trapped in reservoirs below the glacial sediments. However, the sediment fill of pockmarks formed after this event suggests recurrent events throughout the Holocene until today. Most pockmarks occur above folded hydrocarbon-bearing Upper Cretaceous and Paleogene rocks near the western margin of the Magallanes Basin, constraining them as likely source rocks for thermogenic gas.

Introduction

Pockmarks are circular or sometimes elongated crater-like structures within Quaternary sediments of oceans or lakes. They have been first described from an area of the Nova Scotia shelf (King and MacLean 1970), and during the last decades have been detected in many other areas worldwide, in particular along continental margins (e.g., Judd and Hovland 2007; Rise et al. 2015; Roy et al. 2015; Wölfl et al. 2016). The sizes range from <5 m diameter for unit pockmarks to 800 m diameter for giant pockmarks such as the Regab pockmark on the Gabon continental margin (Ondréas et al. 2005). They are thought to originate from explosive expulsion of gas trapped within or below sediments, but apparently can also form during continuous or sporadic migration of fluids or gas along outlet pathways (e.g., Marcon et al. 2013; Maia et al. 2016). Since pockmark fields often indicate thermogenic gas sources, they can be an important exploration tool (Heggland 1998). In some areas they are associated with subsurface hydraulic activity of sediment deposits that may lead to slope failure and seabed instability with subaquatic mass movements (e.g., Judd and Hovland 2007; Moernaut et al. 2017).

This study describes a previously unknown pockmark field in late Quaternary sediments of the Seno Otway fjord (Otway Sound), situated to the east of the southernmost Andes and at the western margin of the Magallanes Basin at 52°S (Figs. 1 and 2). The following formation scenarios can be considered in general. At low temperature and low

✉ R. Kilian
kilian@uni-trier.de

[1] Geology Department, University of Trier, Trier, Germany
[2] University of Magallanes, Punta Arenas, Chile
[3] Bundesanstalt für Geowissenschaften und Rohstoffkunde, Hannover, Germany
[4] Helmholtz-Zentrum für Ozeanforschung, Kiel, Germany
[5] Payloads and Space Sciences Department, INTA, Madrid, Spain
[6] Institute for Baltic Research, Warnemünde, Germany
[7] Alfred Wegener Institute, Bremerhaven, Germany

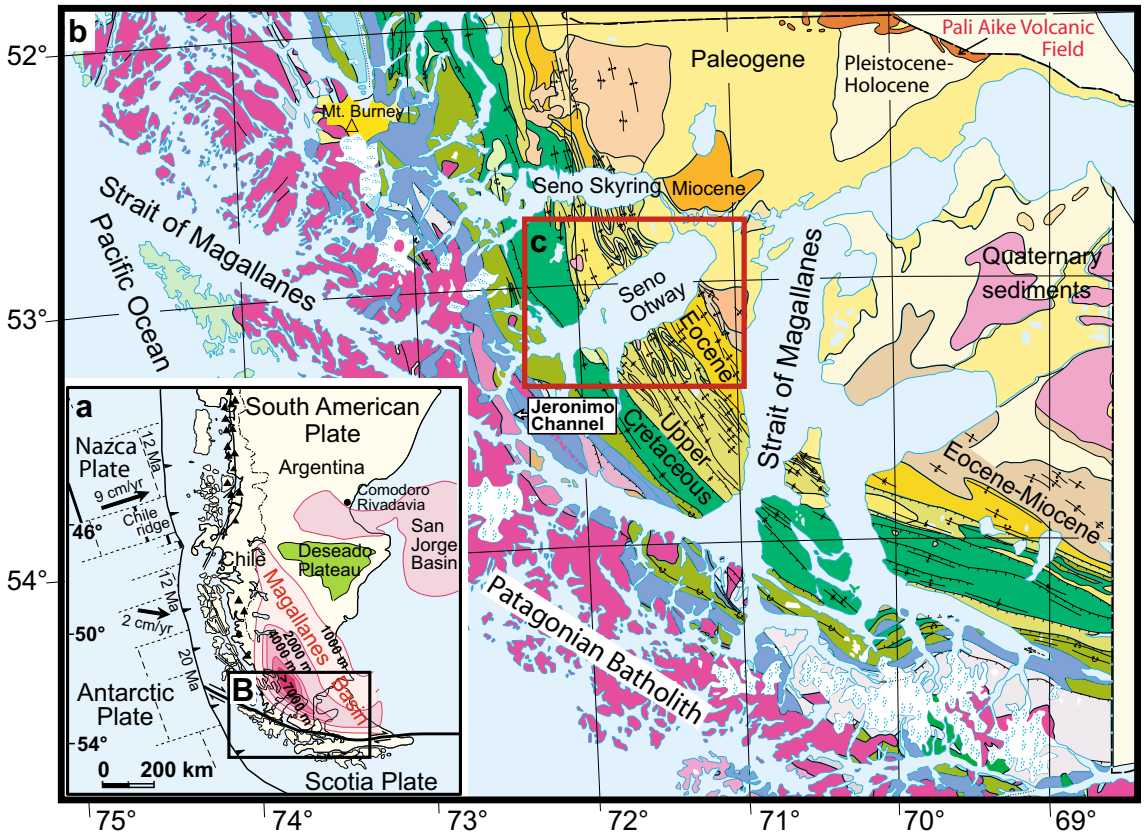

Fig. 1 **a** Plate tectonic framework of the southernmost part of the South American Plate with the oceanic Nazca and Antarctic plates that are subducted with distinct velocities below the Southern Andes. The distribution and sediment thicknesses of the Magallanes and San Jorge basins are after Ramos (1989). **b** Geology of the Magallanes region (cf. Geological map of Chile 1:1 000 000, Sernageomin 2003) with the Upper Cretaceous to Eocene fold and thrust belt forming the southwestern margin of the Magallanes Basin. **c** The Seno Otway fjord region within the fold and thrust belt on the western side of the Magallanes Basin for which more details are shown in Fig. 2

pressure conditions, shallow gas can be formed in sediments by degradation of organic material by microorganisms. Within oceanic sediments at deeper water levels and low temperature, this gas can be also transformed into gas hydrates. Along many continental margins, late glacial warming of the oceans led to decomposition of gas hydrates with associated gas escape (e.g., Portnov et al. 2016) and pockmark formation. Documented examples are the Norwegian continental margin (e.g., Mazzini et al. 2016) and many areas in the Black Sea (e.g., Naudts et al. 2008). To the west of the Patagonian ice field (47°35′S to 50°17′S), Dowdeswell and Vásquez (2013) as well as Dowdeswell et al. (2016) documented pockmarks in three areas of the fjord system and suggested a formation by shallow gas escape. Biogenic gas in sediments is predominantly methane (Hovland et al. 1987; Judd and Hovland 2007), a key greenhouse gas. Thus, such emissions are important for the global atmospheric methane budget and climate development (e.g., Kennett et al. 2003; Krämer et al. 2017).

At greater depth, thermogenic hydrocarbon gas can be formed in suitable source rocks and migrate into reservoirs at 1 to >5 km depth (e.g., Judd and Hovland 2007; Anka et al. 2014; Winsborrow et al. 2016). From there the gas can migrate further upwards along faults or other zones of gas leakage of deep reservoirs, and is then trapped at shallow levels below impermeable caprock sediments in suitable structures (e.g., antiforms). From there the gas can escape in continuous, episodic or explosive ways (Hovland et al. 2002). Gas emissions can be triggered by tectonic events, such as earthquakes (e.g., Cifçi et al. 2003), diapirism, and changes of overburden pressure due to lake- or sea-level changes (e.g., Harrington 1985; Baraza and Ercilla 1996; Judd and Hovland 2007; Duarte et al. 2007; Paull et al. 2008; Riboulot et al. 2013). Occasionally pockmarks are also formed from hydrothermal fluids escaping along fracture zones (Pickrill 1993; Acosta et al. 2001).

Another formation scenario for pockmarks is sediment dewatering (e.g., Harrington 1985; Rise et al. 2015). In particular very thick glacier-proximal sediment units of the late glacial can show forced upward migration of excess pore water, often along active faults and/or topographic highs where the permeability barrier of overlying glacio-lacustrine clays and fine silts is overcome. This scenario may explain the

formation of pockmarks in Lake Villarica, Chile (Moernaut et al. 2017), or near King George Island on the Antarctic Peninsula (Wölfl et al. 2016).

In the light of the above scenarios, this article explores the origin of a newly discovered pockmark field in the Seno Otway in the Magellanes region of Chile. Pockmark distribution, sizes, morphologies, and incision depths were investigated by high-resolution multibeam bathymetry. Parametric sediment echosounding served to visualize the shallow sediment structure around and below the pockmarks. Furthermore, cores were drilled inside and outside of a typical pockmark to document sediment composition and age.

Physical setting

From the Jurassic onwards, the region of the southernmost Andes was a magmatic arc (Hervé et al. 2007; Diaz-Michelena and Kilian 2015) separated from the continental margin of South America by the evolving Magellanes back arc basin (e.g., Calderón et al. 2013). The Magallanes Basin is situated to the east of the southernmost Andes between 49°S and 54°S Fig. 1b). It is 700 km long and 370 km wide, and filled by an up to 8 km thick sediment sequence ranging from the Cretaceous to Quaternary (e.g., Biddle et al. 1986; Ramos 1989; Charrier et al. 2007; McAtamney et al. 2011; Poblete 2015; Malkowski et al. 2015; Betka et al. 2016). Sedimentary rocks on the eastern margin of this basin are exposed to the north (Isla Riesco) and south (Península Brunswick) of the Seno Otway (Figs. 1 and 2).

During the Upper Cretaceous to Paleogene closure of the back arc basin, ophiolites as well as deep-sea and shelf sediments became intensively folded along the eastern slopes of the Andes (e.g., Calderón et al. 2013). They form a NNW–SSE-trending fold and thrust belt that also cross-cuts most of the Seno Otway area (Figs. 1 and 2). The sediments of this period were formed in a coastal marine environment with a high contribution of marine and terrestrial organic matter, making them a source rock for oil and gas. In the Magallanes Basin and Seno Otway area these are mainly marine, littoral and deltaic sandstones (the Cerro Katterfeld, Loreto, Palermo Aike, Río Mayer, Chorillo Chico and Springhill formations; for example, see Urien et al. 1995; Hidalgo et al. 2002; Charrier et al. 2007; Geopark 2010). In addition, coal seams of the Paleogene Magellanes Coal Zone hosted in terrestrial and deltaic sediments are exposed along the northern and southern coasts of the eastern part of the Seno Otway. At present they are mined at the Pecket Mine on the Brunswick Peninsula (Fig. 2; Hidalgo et al. 2002) and the Invierno Mine on Riesco Island (Bustos et al. 2016). The up to 800 m thick sedimentary rocks of the Loreto, El Salto and Palomares formations host the Pecket Mine with numerous 0.3 to 3.0 m thick coal seams. These formations could also represent a possible source rock for thermogenic gas release below glacial sediments.

In the Neogene and up to the present day, the Seno Otway was affected by plate tectonic processes. Up to about 14 Ma, the Pacific oceanic Farallon and Nazca plates have been subducted rapidly (7–8 cm/year) below the South American continent (Fig. 1a). After this the oceanic Chile spreading

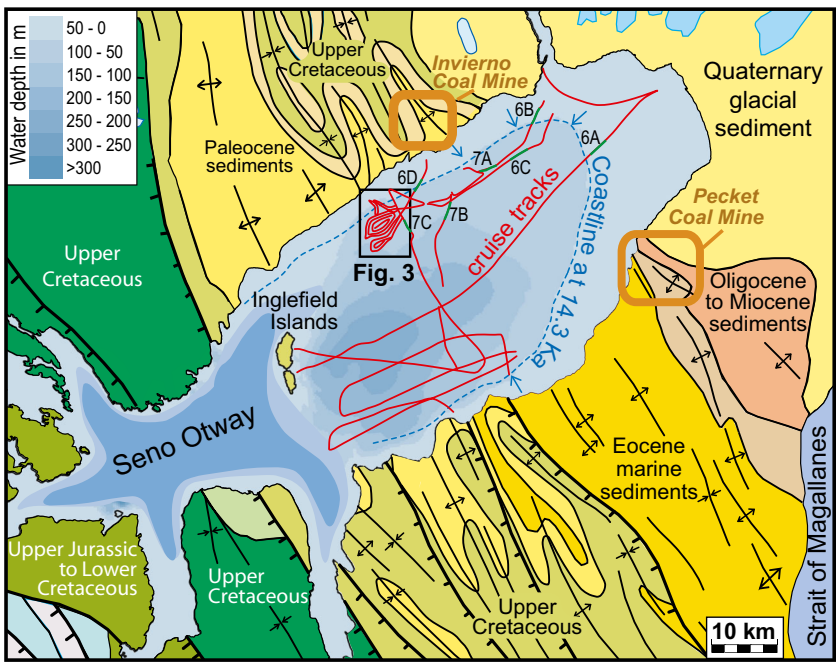

Fig. 2 Bathymetric map of the Seno Otway. *Red lines* Parametric echosounder tracks, *black rectangle* high-resolution multibeam bathymetry (Fig. 3), *numbered green lines* echosounder sections illustrated in Figs. 6 and 7, *blue stippled line* lowering of the coastline by the mega-outflow event at 14.3 ka. Rock lithologies and tectonic lineaments of NNW–SSO-trending fold and thrust belt: geological map of Chile 1:1 000 000 (Sernageomin 2003), Betka et al. (2016), Poblete (2015). *Brownish rectangles* Locations of active Pecket (Hidalgo et al. 2002) and Invierno coal mines (Bustos et al. 2016)

ridge collided with the South American continental margin, and progressively became subducted (Breitsprecher and Thorkelson 2009). Since ridge collision, the Antarctic Plate is obliquely subducted at slow velocities (2–3 cm/year). Related to this oblique subduction, many transform faults formed as well as graben structures in an array oriented nearly perpendicular to the Andean orogen (Fig. 1, e.g., Diraison et al. 1996). These structures constrain the positions and orientations of major fjords (e.g., Glasser and Ghiglione 2009; Breuer et al. 2013). For example, a NNW–SSE-trending dextral fracture zone crosscuts the Seno Otway (Fig. 2). During each glaciation cycle of the Pleistocene, subglacial meltwater streams of the temperate glacier caused a further erosion of the above-described underlying basement. During the glacier retreat from 19.0 to >14.3 ka (e.g., Kilian and Lamy 2012), 15 to 30 m thick glacial sediments have been deposited in the proglacial lake environment of the Seno Otway.

Materials and methods

High-resolution bathymetric data were recorded on board of RV Gran Campo II in March 2008 in the area with the highest density of pockmarks in the Seno Otway (Figs. 2 and 3), with an ELAC Seabeam 1180 multibeam sonar system. Using a frequency of 180 kHz, the system is able to simultaneously record 126 single depth values with a swath up to 153° and is designed for water depths up to 600 m. Depths were calibrated with sound velocity measurements in the complete water column using a CTD48M (Sea & Sun Marine Tech) memory probe. The accuracy of the conductivity and temperature sensor is specified as ±0.003 mS/m and ±0.002 °C, respectively. For geo-referencing and attitude control, the highly sensitive F180R inertial attitude and positioning system from Coda Octopus was used. For further details on the attitude control by these instruments and data processing, see Kjeldsen et al. (2017).

To obtain integrated multibeam and seismic records for visualization of sediment structures, a parametric sub-bottom profiler (SES 96) from Innomar (Wunderlich and Müller 2003) was operated from RV Gran Campo II during different cruises between March 2002 and September 2008 (650 km of cruise tracks; Figs. 2 and 3). The SES 96 can operate in a depth range of 0.5 to 800 m with a vertical resolution of less than 5 cm. The pulse length range is between 0.08 and 1 ms and the beam width is 1.8°. The depths of the sediment surface were calculated from the high-frequency signal and a calibration based on sound velocities obtained from CTD-SD204 (SAIVA/S Environmental Sensors and System) using the post-processing software ISE version 2.9 by Innomar (www.innomar.com). They were used to calculate a low-resolution fjord bathymetry by interpolation with ERSI ArcGIS (Fig. 2). To obtain maximal sediment penetration as well as high spatial resolution, an 8 to 10 kHz beam enabled sediment penetration between 30 and 60 m in water depths up to 600 m.

The echosounder data were edited and recalculated using the post-processing software ISE version 2.9 by Innomar (www.innomar.com). Since propagation of acoustic waves in seawater depends on salinity and temperature, corrections were applied using CTD (conductivity-temperature-depth) profiles taken every 5 to 10 km along the cruise tracks. For depth estimates and interpretation of the echosounder profiles, sediment cores drilled with RV Gran Campo II in 2008 were additionally considered. Locations and depths of the sediment surface layer and important seismic reflectors within the sediment were processed using the geo-information system ArcGIS. Depth values were interpolated based on the Ordinary Kriging method, and used to calculate a bathymetric map.

Based on the high-resolution bathymetry and the parametric echosounder profiles, a typical pockmark was selected among the hundreds identified in the pockmark field (Fig. 3). Pockmark B3 is an elongated feature 110×80 m in length/width and 5 m in depth (see echosounder profile in Fig. 3d). Cores were obtained from aboard R/V Gran Campo II with a 5 m long UWITEC piston corer system (www.uwitec.at). Outside the pockmark and about 40 m from its center, a piston core sampled undisturbed glacial and Holocene sediment (core OTW B3-OUT at 52°57.976′S, 71°40.698′W, 72 m water depth; for location, see Fig. 3). At another coring site inside the pockmark, the sediment infilling was documented (core OTW B3-IN at 52°57.946′S, 71°40.757′W, 77 m water depth). Moreover, 50–70 cm long gravity cores were taken at each location to sample the undisturbed sediment surface. Overlaps with the piston cores were constrained by high-resolution magnetic susceptibility profiles.

Both piston cores contain no macroscopic plant remnants and only very rare, small shell fragments. Thus, the stratigraphy is based on known volcanic tephra layers (Kilian et al. 2003, 2013; Stern 2008). Since thin tephra layers are often not easy to detect in grayish clayey sediments, small peaks along the high-resolution magnetic susceptibility screening (1 mm steps) were considered as first-order indicator for the existence of possible tephra layers. Sediment samples from such layers were analyzed by sieving and microscopic screening as well as with a Leo V435 scanning electron microscope (SEM) at the Geology Department, University of Trier, to detect the texture of glass shards, pumice particles and/or clastic volcanic mineral components. The chemical composition of separated volcanic glass was analyzed by means of atomic absorption spectroscopy at the same department and compared to that of explosive volcanic products of the Aguilera, Reclus, Hudson and Mt. Burney volcanoes, which can be easily discriminated due to their specific chemical signatures (e.g., Stern and Kilian 1996; Kilian et al. 2003, 2013; Stern 2008).

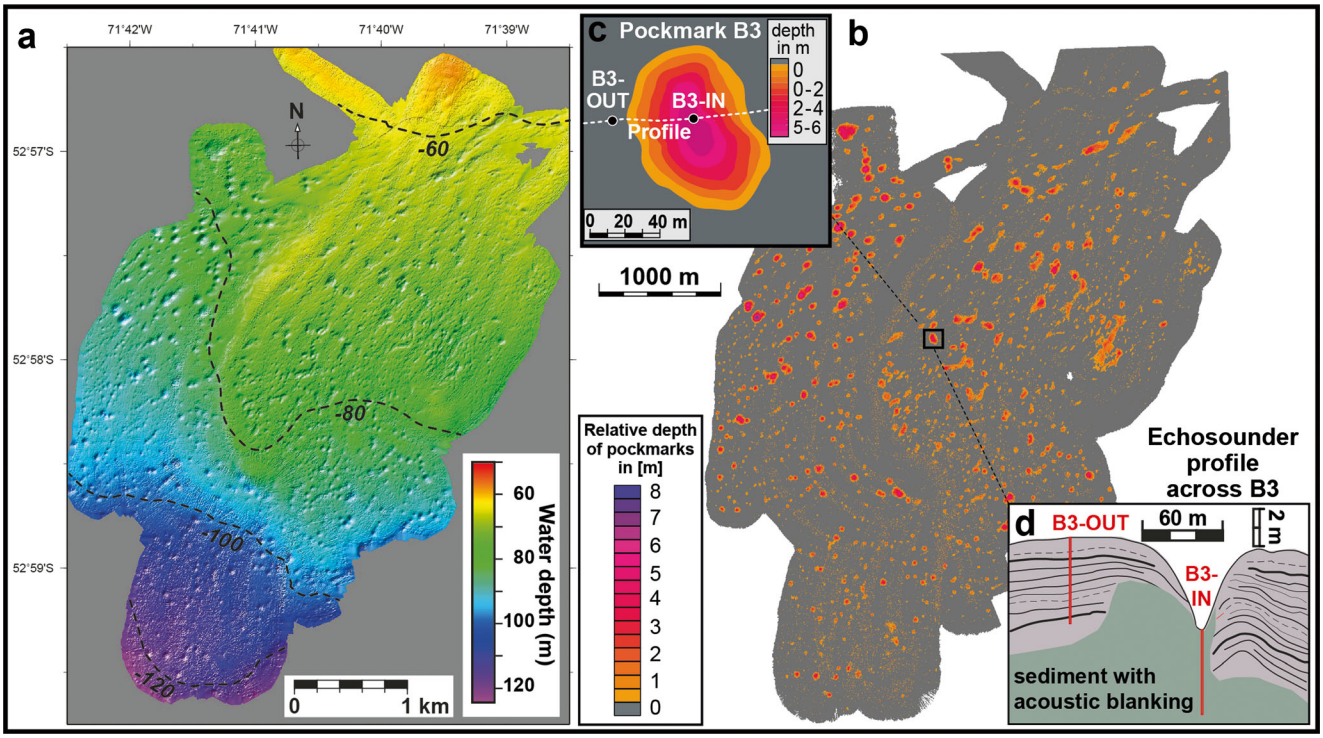

Fig. 3 **a** High-resolution bathymetry mapped during a multibeam survey in September 2008 in the middle section of the northern shore of the Seno Otway (for location, see Fig. 2). **b** Relative depth of pockmarks compared to the smoothed and interpolated sediment surface layer (for mapping area, see Fig. 2). **c** Detailed bathymetry of pockmark B3, with the two coring sites (OTW B3-IN and OW B3-OUT) inside and outside of this pockmark. *White stippled line* Orientation of parametric echosounder profile shown in **d**

One ^{14}C AMS age of 12,950±50 years was determined at NOSAMS (ID: 79833; Woods Hole Oceanographic Institution) from a shell remnant from the lowermost part of core OTW B3-OUT at 438 cm core depth. It was calibrated by using Calib 8.0 and the SHCal13 Southern Hemisphere calibration dataset (Hogg et al. 2013). A reservoir age of 550 years was considered, as determined for sediment core MD-3012 in the Central Strait of Magellan by comparing age/depth relationships with well-dated tephra layers (Kilian et al. 2013; Aracena et al. 2015).

After splitting along the core axes, photographic documentations and descriptions of macroscopic characteristics as well as smear slide analyses were done. Grain size measurements were performed by sieving after dissolution of biogenic carbonate for the >125 μm (fine sand and coarser), 125 to 63 μm (very fine sand), and <63 μm (mud) fractions. Lithic fragments >125 μm were determined and considered as ice-rafted debris (IRD). Additional particle size analyses were made with a Galai CIS-1 laser particle counter with an analytical range between 0.5 and 150 μm. About 50 mg of air-dried sediments were dissolved in 50 ml distilled water. Carbonate was dissolved and organic material was removed with a solution of H_2O_2 (10%) over a period of 15 h. Afterwards the samples were placed in 60–70 °C water bath. Finally, the samples were treated in an ultrasound bath for 20 min. These data were used to calculate clay/silt ratios (clay 0.5–2 μm; silt 2–63 μm).

Magnetic susceptibilities were measured at the Institute for Baltic Research (IOW) in Warnemünde, Germany, with a Bartington MS2E core logging system at a frequency of 2 kHz and 1 mm steps along core intervals. This involved integrating an area of 3.8×10.5 mm for each sediment surface measurement.

Total carbon (TC), total nitrogen (TN) and total organic carbon (TOC or C_{org}) were measured with a Vario EL III CHNOS elemental analyzer at IOW. Before analysis, all samples were freeze-dried and homogenized using an agate mortar and pestle. Calcium carbonate was calculated as $CaCO_3 = (TC–TOC)×8.333$, where TC is the total carbon content of untreated samples and TOC is the total organic carbon content of HCl-treated samples. N/C ratios were used to estimate aquatic versus terrestrial endmembers of organic carbon. Indeed, it has been shown that mixing equations based on C/N ratios underestimate the terrestrial fraction, whereas N/C ratios provide a linear relationship between both sources (Perdue and Koprivnjak 2007). The considered molar N/C ratio endmembers for marine microalgae is 0.17 (C/*N*=6), and for terrestrial plants it is 0.033 (C/*N*=30.6), both taken from Lamy et al. (2010).

The elemental composition of cores OTW B3-IN and OTW B3-OUT as well as the considered uppermost gravity core section was assessed in situ with an Avaatech™ X-ray fluorescence (XRF) core scanner at Alfred Wegener Institute (AWI), Bremerhaven, Germany. This non-destructive technique provides semi-quantitative geochemical analyses of split sediment cores with a resolution of <1 cm (Rothwell and Rack 2006). Measurements were carried out with a rhodium anode, a voltage of 10 kV and current range at 0.3 mA. No filter was used. Si, Ti, Al, Mn, Fe, Ca, K, S and Cl were measured but only Cl, Ca/Ti, K/Ti and Al/Si ratios are reported in this study.

Results

The stratigraphy and age control points of the 494 cm long sediment core OTW B3-OUT is illustrated in Fig. 4, based on the following tephra layers with well-known ages: the 2.05 ka Mt. Burney tephra (53 cm core depth), the 3.1 ka Aguilera tephra (77 cm), the 4.15 ka Mt. Burney tephra (115 cm), and the 9.3 ka Mt. Burney tephra (248 cm; see Kilian et al. 2003, 2013; Stern 2008). A shell fragment at 438 cm core depth gave a ^{14}C age of 12,950±50 years (14.78 ka). Due to the paucity of shell fragments and foraminifera, no further ^{14}C ages could be obtained.

In core OTW B3-OUT, a marked compositional change between 425 and 420 cm core depth (in, for example, chlorinity as well as Ca/Ti and K/Ti ratios) is associated with a marine transgression that occurred at ~14.3 ka (Kilian et al. 2013). Another pronounced change at 200 cm core depth is probably related to strong variations in paleoclimate conditions (lower precipitation, weaker westerlies and lower temperatures), as documented also in many other fjord sediment cores from the Magellanes region and dated to about 8.2 ka (Lamy et al. 2010; Kilian and Lamy 2012; Kilian et al. 2013). The above-described stratigraphical framework indicates plausible and relatively constant sedimentation rates during the late glacial and Holocene ranging from 25 to 35 cm/1,000 years at the Seno Otway (Fig. 4).

In core OTW B3-OUT, the lowermost section from 492 to 435 cm core depth (>14.3 ka) is characterized by the lowest values of chlorinity and Ca/Ti ratios (indicative of low biogenic carbonate contents; Fig. 4) as well as by relatively high clay/silt ratios of 0.5 to 0.8. Foraminifera are absent and C_{org} contents are very low (<0.6 wt%). All this is consistent with sedimentation within a proglacial lake.

Between 425 and 420 cm core depth (ca. 14.3 ka), the strong increase in chlorinity values and Ca/Ti ratios suggest a first marine transgression (see above). Ratios of K/Ti and Al/Si also increase significantly above 430 cm core depth, reaching maximum values at ~390 cm. Further up-core, these values drop progressively up to 200 cm core depth (equivalent to 8.2 ka). In the uppermost 200 cm of core OTW B3-OUT, the K/Ti and Al/Si ratios remain low. Highest chlorinity values and Ca/Ti ratios occur between 270 and 220 cm core depth (ca. 10.0–9.0 ka).

The whole core section between 492 and 200 cm is characterized by C_{org} contents lower than 0.6 wt%. Further up-core, C_{org} contents increase progressively to as much as 1.1 wt% during the last 8 ka, probably reflecting a slight enhancement of bioproductivity (Ríos et al. 2016). Increasing contribution of terrestrial C_{org} is indicated by lower N/C ratios above 350 cm core depth and in particular in the uppermost

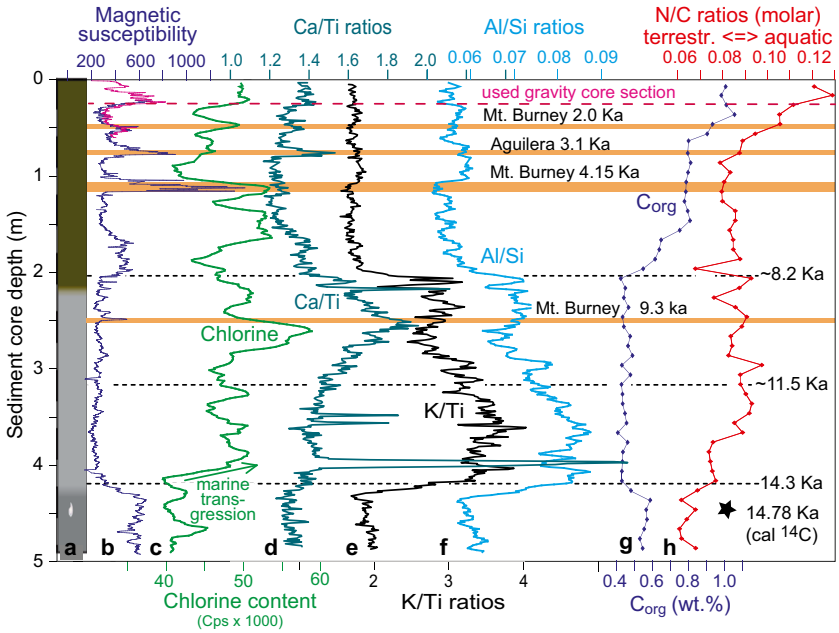

Fig. 4 Sedimentological and chemical characteristics of core OTW B3-OUT from outside of pockmark B3 (see location in Fig. 3c, d), revealing three lithologies with distinct colors (a), magnetic susceptibilities (b), chlorine contents (c), Ca/Ti ratios as indicator for biogenic carbonate (d), K/Ti ratios documenting illite-rich allochtonous sediment from the Patagonian Batholith located to the west (e), Al/Si ratios as indicator for grain size variations, C_{org} contents (f), and N/C ratios (molar) characterizing terrestrial versus aquatic organic carbon (g). Magnetic susceptibility is shown in pink with the stippled line indicating the uppermost section from the corresponding gravity core

70 cm (i.e., during the last 2 ka). This core section is also characterized by relatively low clay silt ratios of 0.1 to 0.5.

Sediment core OTW B3-IN does not contain tephra layers that could be used as age markers (Fig. 5). Also, there is no biogenic carbonate suitable for ^{14}C age determinations. Its stratigraphy with IRD-bearing layers cannot be correlated with stratigraphical features of core OTW B3-OUT or other sediment cores from the Magellan region (for compilation, see Kilian et al. 2013). Therefore, it is suggested that the sediments within this pockmark represent a mixture of glacial sediments that were disrupted and re-deposited during late Holocene pockmark formation and activity.

Between 470 and 70 cm depth, core OTW B3-IN is characterized by clay/silt ratios of 0.4 to 0.9. Two laminated sections appear at 415–360 and 290–250 cm, incorporating several IRD layers (Fig. 5) with very low C_{org} contents (<0.3 wt%). The appearance of abundant IRD as well as the range of chlorinity contents and Ca/Ti ratios of this core section is similar to those of the proglacial lake stage in core OTW B3-OUT below 430 cm core depth (Fig. 4). Between 470 and 70 cm, the K/Ti and Al/Si ratios are also typical for glacial sediments, indicating that this unit represents exclusively reworked glacial sediments. From 70 to 0 cm core depth, the chlorinity and Ca/Ti ratios increase significantly, indicating marine conditions with some biogenic carbonate (Fig. 5). Thus, the uppermost 20 cm of both cores OTW B3-IN and OTW B3-OUT have similar chlorinity values as well as Ca/Ti and Al/Si ratios, suggesting coeval deposition during the last 1,000 years.

A total of 650 km parametric echosounder profiles was surveyed to the east of the Ingelfield Islands in the Seno Otway in water depths of <20 to 250 m (tracks shown in Fig. 2). Most pockmarks occur at water depths between 100 and 50 m. Abundances range from 5 to >20 per kilometer of echosounder profile. Directly below and/or next to the pockmarks, acoustic masking is often observed in the underlying sediments (Figs. 6 and 7). Sediment doming, a typical morphological feature beneath the pockmarks, would be caused by trapped upward-migrating gas sealed by glacial clay horizons. Vertical pipes of acoustic masking indicate gas chimneys, which range from the acoustic basement through the whole Quaternary sediment sequence up to the surface, in particular close to the pockmarks (Figs. 6 and 7). The occurrence of pockmarks is almost always related to normal or strike-slip faults, which affect the whole sedimentary sequence down to the acoustic basement. Often the echosounder profiles do not cross the centers of pockmarks. Thus, total thickness of the sediment infill cannot be determined with confidence.

Figure 6 shows E–W-oriented echosounder profiles at water depths of ~50, ~65, 62–75, and 75–80 m. In the two shallower profiles the slightly folded glacial sediments are truncated by erosional surfaces, which are indicated by strong reflectors. These surfaces are discordantly overlain by a 2–4 m thick sediment sequence. Commonly, buried paleo-pockmarks occur directly below this erosional unconformity, while some pockmarks also cut into this uppermost sequence, which is probably of late glacial and Holocene age. The two profiles from water depths greater than 60 m show the same pronounced reflector at 3–5 m sediment depth, but the underlying glacial sediments are more concordant. The profile in Fig. 6d reveals buried and non-buried paleo-pockmarks above

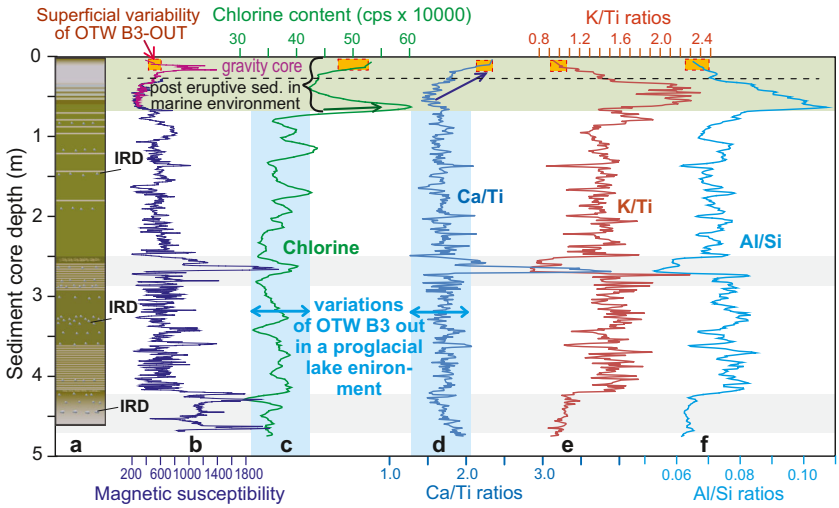

Fig. 5 Sedimentological and chemical characteristics of core OTW B3-IN from inside of pockmark B3 (for location, see Fig. 3), revealing lithological units with IRD and laminated sectors (a), magnetic susceptibilities (b), chlorine content (c), Ca/Ti ratios as indicator for biogenic carbonate (d), K/Ti (e), and Al/Si as indicator for glacial clay (f). *Vertical blue bars* Range of chlorinity and Ca/Ti ratios within the lowermost section of core OTW B3-OUT (490 to 425 cm core depth) for which a proglacial lake environment is assumed. Post-eruptive sediment fill is marked above 70 cm core depth. The section taken from a gravity core is indicated

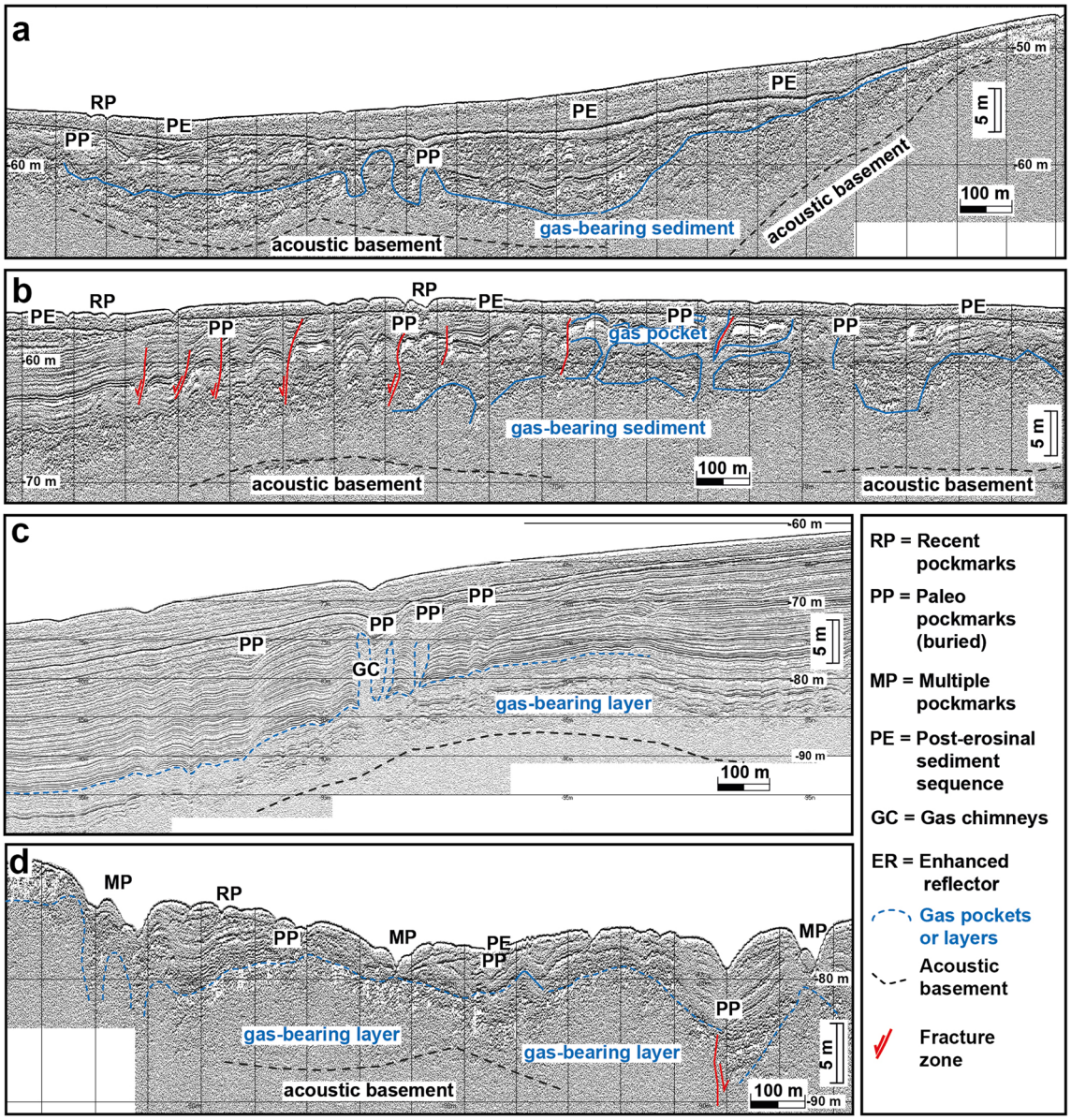

Fig. 6 W–E-oriented echosounder profiles of the Seno Otway, with water depths increasing from **a** to **d**. **a** Up to 10 m thick slightly folded glacial to late glacial sediment sequence at 47 to 53 m water depths above gas reservoirs and associated paleo-pockmarks. The surface of these layers was discordantly eroded, and is overlain by a pronounced reflector and 3–5 m thick post-erosional sediments deposited after ~14.3 ka. **b** Folded glacial sequence at ~65 m water depths with neotectonic faults with buried paleo-pockmarks and underlying gas reservoirs. Post-erosional sediments are 1.5 to 2.0 m thick and include some recent pockmarks (*RP*). **c** 20 m thick late glacial and Holocene sediments with buried paleo-pockmarks. Note: the erosional discordance is less pronounced than at the shallower sites in **a** and **b**. **d** Example of buried and unburied paleo-pockmarks, multiple and recent pockmarks within 10 m thick glacial sediments and above gas reservoirs and an acoustic basement

gas pockets and the acoustic basement. More recent pockmarks with single and multiple structures cut up to 10 m deep into Holocene and glacial sediments.

Figure 7 shows three different echosounder profiles surveyed in 75 to 85 m water depth, also within the extended pockmark field shown in Fig. 3. Recent pockmarks are 4 to 8 m deep and have post-eruptive sediment infills of 0.1 to 2 m thickness (for example, see Fig. 3d). The pronounced reflector marking the erosional unconformity at shallower sites (see above) is again more or less concordant at greater water depths. Overlying late glacial and Holocene sediments have thicknesses of 3 to 5 m. The glacial sediment sequence is 20 to >25 m thick and characterized by numerous parallel seismic reflectors. Sediments of 10 to >15 m thickness with a less well-defined acoustic stratification occur below the bottom of the glacial sequence and above the acoustic basement. Acoustic blanking appears also in some sediment layers

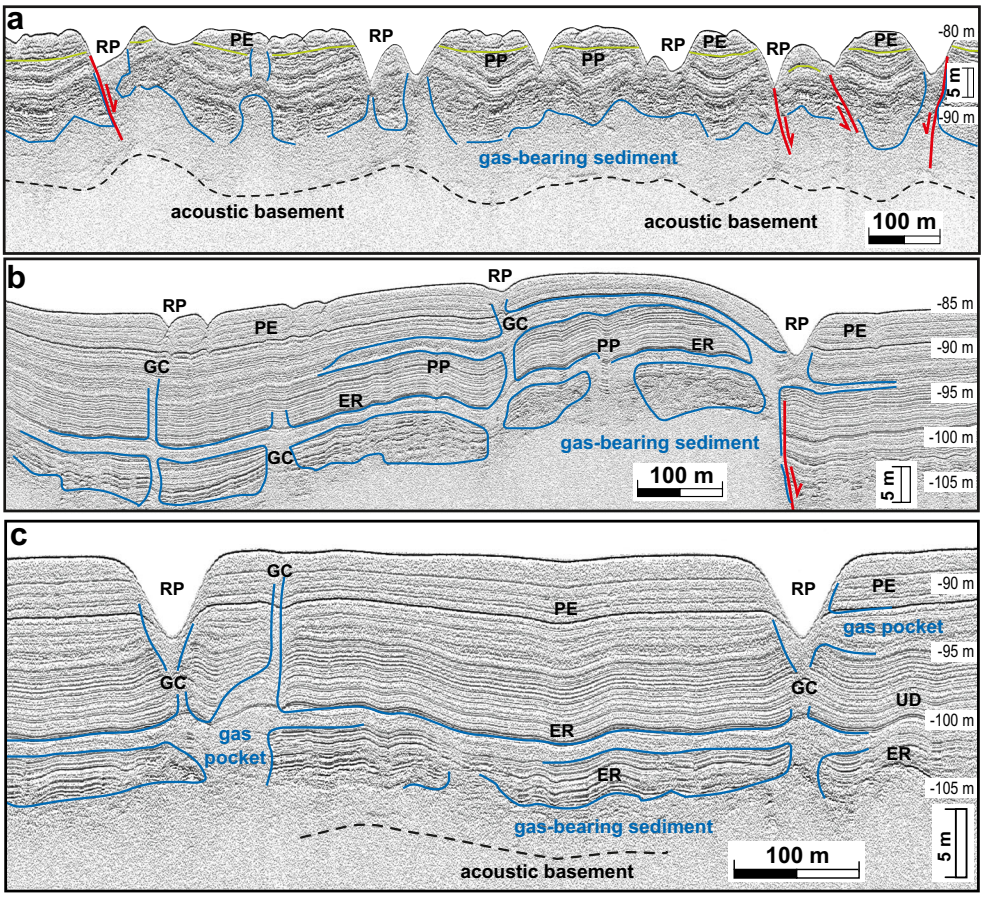

Fig. 7 **a–c** Echosounder profiles of the Seno Otway (for locations, see Fig. 2) with examples of various up to 7 m deep pockmarks within 15 to >20 m thick glacial and Holocene sediments at water depths of 75 to 90 m. The amount of post-eruptive sediment infill differs depending on the period after the last gas eruption. The pronounced seismic reflector at 3 to 5 m sediment depth, which marks the post-erosional (*PE*) discordance at the shallower sites of Fig. 6, is concordant at these deeper sites. The acoustic basement is reached at about 25 m sediment depth. Enhanced reflectors (*ER*) and acoustic turbidity indicate gas reservoirs. Upward flexures of sediment layers above these reservoirs indicate updoming and are associated with vertical gas chimneys (*GC*) that occur in particular below the pockmarks

below strong reflectors, indicating gas pockets and gas-bearing sediments within probably coarser clastic glacial layers. Some recent pockmarks are situated above active faults. Like in the four profiles of Fig. 6, sediment doming and gas chimneys represent common features associated with numerous pockmarks.

The area with the highest pockmark abundance (16 to 31 pockmarks per km^2) is found along the northern shores of the Seno Otway in 60 to 80 m water depths (Fig. 3a). Here, a high-resolution multibeam bathymetric map covering approx. 40 km^2 about 25 km SW of the Invierno Coal Mine on Riesco Island (Figs. 2 and 3) reveals up to 10 m deep and 150 m wide pockmarks resembling funnel- and/or crater-like depressions within the uppermost Holocene and late glacial sediment layers. Figure 3b shows their distribution and their relative depressions compared to a calculated, flat sediment surface. They have variable forms, and can be classified as standard circular, elliptical and asymmetric pockmarks, unit pockmarks and elongated pockmarks, whereas composite or eyed pockmarks as well as pockmark strings were not detected. Beside this high-density pockmark area, sparsely distributed pockmarks were detected along the other echosounder profiles (Figs. 2, 6 and 7). However, a clear alignment of the pockmarks along possible N–S-trending fracture zones was not observed (cf. Breuer et al. 2013). The highest density of 16 to 31 pockmarks per km^2 occurs 4.5 km from the northern shore of the Seno Otway, where slightly folded Paleocene and Upper Cretaceous sedimentary rocks crop out, representing the margin of the Magellanes Basin (Fig. 2).

Discussion

To constrain the timing of late glacial and Holocene pockmark formation in the Seno Otway, a combination of stratigraphical and compositional characteristics of the two sediment cores within and outside of pockmark B3 as well as sediment structures from the echosounder profiles were considered. The late glacial sedimentation rate of the well-stratified and undisturbed core OTW B3-OUT was ~40 cm/1,000 years from 14.3 to 11.6 ka. The early Holocene sedimentation rate was ~30 cm/1,000 years, and the last 8.5 ka are characterized by relatively constant sedimentation rates of 25 cm/1,000 years (see Fig. 4). This is similar to sedimentation rates found in the SK1 sediment core from the eastern Seno Skyring (Fig. 2; Kilian et al. 2007a, 2013). However, core OTW B3-OUT shows a strong compositional change at 430 to 420 cm core depth at about 14.3 ka. This compositional change is probably

coeval with the erosional unconformity in the sediment echosounder profiles from the eastern Seno Otway at water depths of less than 60 m (Fig. 6; see also Kilian et al. 2013).

This interpretation implies that the glaciers retreated from Jeronimo Channel at about 14.3 ka (as previously suggested and dated by Mercer 1982) and opened a new water outflow pathway from the Otway towards the Strait of Magellan (see Fig. 1). This probably led to a very large outflow event of this proglacial lake (320 km^3), and a lake level lowering from 20 m above sea level (as documented by paleo-terraces around the Seno Otway) by about 80 m, i.e., to –60 m relative to the present-day sea level (Kilian et al. 2013). Figure 2 shows the large area in the middle and eastern sector of the Seno Otway that became exposed to fluvial erosion and sediment re-deposition in deeper fjord areas. The reworked glacial sediments have relatively high illite/chlorite, K/Ti and Al/Si ratios since they are derived from granitoid rocks of the Patagonian Batholith exposed to the west of the coring site in the Andean mountains. Similar sediments were also deposited in the Seno Skyring during the late glacial period (Kilian et al. 2007a, 2013).

After the outflow event, a marine transgression (Fig. 1; Kilian et al. 2007b) proceeded with the ongoing global sea-level rise until ~8 ka. In addition, reduced precipitation after 9 ka (Lamy et al. 2010) diminished the contribution of sediments with a glacial clay signature (high K/Ti and high Al/Si ratios) in the eastern Seno Otway, as documented in core OTW B3-OUT from 400 to 200 cm sediment depth (~14.0 to 8.2 ka; Fig. 4), while K/Ti and Al/Si ratios remained relatively low and constant during the last 8 ka.

The above-described lithological transition at about 14.3 ka, and the 4.15 ka Mt. Burney tephra layer represent two well-defined reflectors in many of the echosounder profiles (Figs. 3d, 6 and 7). These reflectors were therefore also used to constrain regional changes in sedimentation rates. Depending on the regional sedimentation rates, the pronounced late glacial transition is imaged as a strong reflector in 2 to 5 m sediment depth in the echosounder profiles (examples shown in Figs. 6 and 7).

The sediment depths in which the 4.15 ka Mt. Burney reflector appears indicate a general decrease in sedimentation rates in the Seno Otway from west to east towards shallower sites (see also from Fig. 6a to d), like also documented for the Seno Skyring fjord by Kilian et al. (2007a). Next to Ingelfield Island in the middle of the Otway fjord system at about 200 m water depth (Fig. 2), the echosounder profiles show the 4.15 ka Mt. Burney tephra layer in up to 2 m sediment depth, corresponding to a high sedimentation rate of 50 cm/1,000 years). This suggests a long-term sediment redistribution into the deeper parts of the fjord basin. From Ingelfield Island towards the shallow eastern fjord shores, average late Holocene sedimentation rates decrease from <50 to <15 cm/1,000 years. Towards the southern and northern coasts, sedimentation rates decrease to <25 cm/1,000 years. Because of these regional variations, the thicknesses of undisturbed sediment deposition outside of the pockmarks were compared with the post-eruptive inside filling to estimate the ages of its last activity. The results indicate a more or less continuous activity spectrum during the last 14 ka for the pockmark field. The analyzed relative thicknesses of the sediment fillings of different pockmarks suggest a formation and/or ongoing activity throughout most of the Holocene. In the case of the drilled pockmark B3, only the upper 20 cm of core OTW B3-IN from the center of the pockmark are comparable to that of core OTW B-OUT (Fig. 4). This indicates that this pockmark was formed and/or was still active until about 1.0 ka. The variations of IRD content and sediment laminations in pockmark B3 indicate multiple eruptions and sediment re-deposition phases.

The Andean glacier front probably retreated from the easternmost shorelines of the Seno Otway coeval to that of the Seno Skyring at about 18 ka (Kilian et al. 2007a, 2013; Kilian and Lamy 2012). This constrains a maximum age of the older pockmarks. However, many buried and/or partly eroded paleo-pockmark structures are visible in the profiles of Fig. 6 within the glacial sediment sequence directly below the strong reflector marking the erosional unconformity. It is documented from many coastal areas worldwide that changes in sea level and corresponding changes in hydrostatic pressure can promote pockmark formation (e.g., Harrington 1985; Baraza and Ercilla 1996; Judd and Hovland 2007; Duarte et al. 2007; Paull et al. 2008; Riboulot et al. 2013). During the mega-outflow event of the Seno Otway (see above), hydrostatic pressure probably was reduced by about 50% within a few weeks. It is inferred that this caused gas expulsions and pockmark formation as documented in the echosounder profiles of Figs. 6 and 7. It is possible that some of these paleo-pockmarks were totally eroded after aerial exposure at a level above 60 m water depth. After reaching present-day sea levels at around 6 ka, the coastline and the hydrostatic pressure experienced little changes.

Factors influencing the morphology of pockmarks are spatial differences in sediment accumulation, geometry of subsurface bedding, availability of migration paths (fractures and faults), differences in expulsion rates, and action of bottom currents (e.g., Judd and Hovland 2007; Roy et al. 2015; Maia et al. 2016). Pockmarks of the Seno Otway are mainly circular, but some are also elongated in a W–E direction. The latter occur particularly in areas of shallower water depth and could have been shaped by wind-induced currents in the upper water column of less than 65 m water depth (Fig. 3b). Some constraint for this comes from the documented thermohaline structure in the

Seno Skyring (Kilian et al. 2007a) and Seno Otway (Kilian et al. 2013). Such wind-induced currents were considered as causes for elongated pockmarks next to Spitzbergen glaciers (Roy et al. 2015).

Diameter/depth ratios of 10 to 60 with an average of 23 characterize the 220 morphometrically analyzed pockmarks of the Seno Otway. Since the echosounder profiles do not always cross the pockmark centers, these estimates must be interpreted with care. In general, however, the results indicate that many pockmarks have relatively steep inner slopes, and are relatively young without significant sediment infill and/or erosion at the rims. Many observed pockmarks from other regions in the world have higher diameter/depth ratios—e.g., Belfast Bay (Andrews et al. 2010), the inner Oslo Fjord (Webb et al. 2009) and the Scotian Shelf (Fader 1991). The widening of pockmark diameter can be attributed to reduced sealing capacity caused by thin overlying marine sediment layers. In contrast, pockmarks with smaller diameters relative to their depths—like those of the Seno Otway—have been found in Isfjorden (Roy et al. 2015). Most of these relatively "deep pockmarks" (diameter/depth <30) have been identified along ridges and are interpreted as seafloor expressions of bedrock outcrops and thrust faults that provide either organic-rich source rocks and/or migration pathways for fluids to the pockmarks (Roy et al. 2015).

The area with the highest density of pockmarks (19 to 31 pockmarks per km^2) is located between 50 and 95 m water depth in the northern part of the Seno Otway about 25 km southwest of the Eocene lignite outcrops of the Mina del Invierno on Isla Riesco (Figs. 2 and 3). This is among the highest density of pockmarks reported worldwide (cf. Maia et al. 2016). Bedrock units that crosscut the Seno Otway within the area of highest pockmark density include slightly folded Upper Cretaceous-Paleocene sediments (McAtamney et al. 2011; Betka et al. 2016). These were formed in a marine environment and near the earlier marine shelf edge (see Introduction), and were probably tectonically overlain by Late Eocene and Miocene sediments including deposits of the Magellan Coal belt (Bustos et al. 2016). The echosounder profiles of the present study also show that many pockmarks are located above deep-reaching faults (Figs. 6 and 7).

Areas with more than 100 and up to 200 m water depths and glacial sediments thicker than 50 m have only few pockmarks. These zones are characterized by much higher overburden pressure from the water column and much thicker glacial sediments, which may reduce the capacity of metastable underlying gas reservoirs to migrate and erupt at the seafloor.

The C_{org} contents of the late glacial and early Holocene sediment core section range from 0.4 to 0.6 wt%. N/C ratios of 0.08 indicate that more than 60 wt% of the organic matter is derived from terrestrial sources when suggesting a typical aquatic and terrestrial plant endmember of fjord sediment cores from the investigated fjord system (Lamy et al. 2010). Between 14 and 4 ka there is no significant change in C_{org} content in core OTW B3-OUT, indicating that there was little or no long-term degradation. In both sediment cores from inside and outside pockmark B3, there was no evidence of extension voids typical for pore fluid outgassing in the sediment during core extraction and elevation. Furthermore, no H_2S smell was detected, arguing against gas formation by anoxic decomposition of sedimentary organic carbon. Even in many areas of the Magellanes fjords where the late glacial and Holocene sediments have much higher C_{org} contents of up to 30 wt%, high densities of pockmarks have not been detected (Kilian et al. 2007a, 2013; Breuer et al. 2013; Fernández et al. 2017). In addition, echosounder profiles along the Seno Skyring (Kilian et al. 2007a; Breuer et al. 2013), which crosscut a lithological belt similar to the Seno Otway (McAtamney et al. 2011; Schwartz and Graham 2015; Bustos et al. 2016), showed only few isolated and small pockmarks. Furthermore, the sedimentological properties of the SKY 1 sediment core, located along an E–W-oriented echosounder profile in the Seno Skyring, do not indicate shallow gas formation (Kilian et al. 2007a). Thus, it is suggested that possible shallow gas sources, as proposed for pockmarks in the fjords to the west of the Southern Patagonian Ice field (Dowdeswell and Vásquez 2013), are of minor importance for the origin of most of the Seno Otway pockmarks.

As described above, the highest densities of pockmarks occur above the subcrop of the Late Cretaceous and Tertiary fault and thrust belt (Fig. 2). In addition, echosounder profiles across pockmarks often show swelling and doming structures within the sediment layers of low permeability, indicating metastable shallow gas-bearing sediment layers probably sourced from deeper rock lithologies (e.g., Cifçi et al. 2003). Furthermore, gas chimneys penetrate through the whole Quaternary sediment sequence and are often next to fracture zones within the acoustic basement (Fig. 7). Thus, deeper thermogenic gas sources need to be considered. They include Upper Cretaceous (Rosa unit) and lower to middle Tertiary formations (Agua Fresca and Chorillo Chico units), which are weakly metamorphosed sediments formed in a back arc basin and continental shelf environment. These up to 2,000 m thick units contain potential source rocks of thermogenic hydrocarbon gas (Geopark 2010; McAtamney et al. 2011; Schwartz and Graham 2015; Bustos et al. 2016). Such gas could have been trapped in anticlinal structures formed by over-thrusting and folding at the western margin of the Magallanes Basin.

Younger coal-bearing Cenozoic sediments may be another source for thermogenic gas. Several coal seams of 0.3 to 3.0 m thickness occur in up to 800 m depth within sedimentary units of the Loreto (Oligocene to Miocene), El Salto (Miocene) and Palomares (Miocene) formations at the eastern margin of the Magallanes basement (Hidalgo

et al. 2002). At present these coal deposits are mined in the Pecket Mine on the southeastern shores of the Seno Otway (Fig. 2) and the Invierno Mine on Riesco Island just 25 km northeast of the observed major pockmark field. The coal seams occur in an overall paralic succession developed in a marine deltaic to lagoonal depositional setting (Mella 2001), i.e., in a rheotrophic hydrogeological environment with peat formation and an aquatic/herbaceous vegetation, and with very low oxidation levels of underlying soils. The volatile components of the coal amount to 41 vol% on average. Thus, these sediments are another source of thermogenic gas. However, only seismic profiles with a deeper penetration across the Seno Otway will be able to constrain these potential source rocks.

An origin of pockmarks by expulsion of thermogenic gas has also been suggested for other coastal areas. For example, Roy et al. (2015) showed that the combined presence of fault conduits, potential source rock, and thin postglacial sediment cover is crucial for the formation of thermogenic gas and associated pockmarks at Isfjorden in the Svalbard region. In Nordfjorden, inner Isfjorden and parts of Sassenfjorden, about 50% of the pockmarks lie on thermogenic gas-bearing Upper Permian–Lower Jurassic strata (Bælum and Braathen 2012). Michelsen and Khorasani (1991) also documented the relationship of pockmark formation and large amounts of Tertiary gas generation from the Lower Carboniferous coals. Usually gas is stored in coal seams in the form of coal bed methane (Scott 2002). However, this methane gas can be desorbed and released following post-glacial rebound, leading to seepage at the seafloor and the formation of pockmarks.

Conclusions

1. An extensive and probably still active late Quaternary pockmark field in the Seno Otway of the Magallanes region, Chile has been documented by multibeam bathymetric and parametric echosounder data. Apparently thermogenic gas was trapped in coarse-grained sediment pockets and layers below relatively impermeable clayey glacial sediments of 15 to >30 m thickness. Sediment cores from the uppermost 5 m give no implications for significant gas release from shallow sediments.
2. The locations of the pockmarks are constrained by fracture zones of Neogene age that connect to underlying Cretaceous and Cenozoic sediment sequences at the folded Western Margin of the Magellanes Basin. Because these rocks are coal-bearing, they are the likely source of thermogenic gas. However, only deeper seismic investigations will be able to better constrain the architecture of the fold and thrust zone, and the link to potential source rocks.
3. Many of the documented pockmarks probably formed after a postglacial mega-outflow event associated with a 80 m lowering of the water level of the Seno Otway at 14.3 ka. Although more precise dating is required, this study highlights the overall sensitivity of gas release from sediments in response to changes in water levels.

Acknowledgements This study was funded by Grant Ki-456/11 of the German Research Foundation (Deutsche Forschungsgemeinschaft, DFG). We thank Willi Weinrebe (Geomar, Kiel) for his assistance in setting up the portable multi beam equipment, and Marcelo Arevalo for his encouragement during various cruises aboard the RV Gran Campo II since 2002, Dr. Carlos Ríos from the University of Magallanes for a multiple logistic support, and Francisco Ríos for assessing a preliminary version of the manuscript. Also acknowledged are very constructive suggestions from the journal editors and an anonymous reviewer.

Compliance with ethical standards

Conflict of interest The authors declare that there is no conflict of interest with third parties.

References

Acosta J, Muñoz A, Herranz P, Palomo C, Ballesteros M, Vaquero M, Uchupi E (2001) Pockmarks in the Ibiza Channel and western end of the Balearic promontory (western Mediterranean) revealed by multibeam mapping. Geo-Mar Lett 21:123–130

Andrews BD, Brothers LL, Barnhard WA (2010) Automated feature extraction and spatial organization of seafloor pockmarks, Belfast Bay, Maine, USA. Geomorphology 124(1-2):55–64. https://doi.org/10.1016/j.geomorph.2010.08.009

Anka Z, Loegering MJ, di Primio R, Marchal D, Rodríguez JF, Vallejo E (2014) Distribution and origin of natural gas leakage in the Colorado Basin, offshore Argentina margin, South America: seismic interpretation and 3D basin modelling. Geol Acta 12(4):269–285

Aracena C, Kilian R, Lange CB, Bertrand S, Lamy F, Arz H, DePol-Holz R, Pontoja S, Kissel S (2015) Holocene variations in productivity associated with changes in glacier activity and freshwater flux in the central basin of the strait of Magellan. Palaeogeogr Palaeoclimatol Palaeoecol 436:112–122. https://doi.org/10.1016/j.palaeo.2015.06.023

Bælum K, Braathen A (2012) Along-strike changes in fault array and rift basin geometry of the carboniferous Billefjorden trough, Svalbard, Norway. Tectonophysics 546-547:38–55. https://doi.org/10.1016/j.tecto.2012.04.009

Baraza J, Ercilla G (1996) Gas-charged sediments and large pockmark-like features on the Gulf of Cadiz slope (SW Spain). Mar Pet Geol 13(2):253–261. https://doi.org/10.1016/0264-8172(95)00058-5

Betka P, Klepeis K, Mosher S (2016) Fault kinematics of the Magallanes-Fagnano fault system, southern Chile; an example of diffuse strain and sinistral transtension along a continental transform margin. J Struct Geol 85:130–153. https://doi.org/10.1016/j.jsg.2016.02.001

Biddle KT, Uliana MA, Mitchum M Jr, Fitzgerald MG, Wright RC (1986) The stratigraphic and structural evolution of the central and eastern Magallanes Basin, southern South America. In: Allen PA, Homewood P (eds) Foreland basins. Int Assoc Sedimentol Spec Publ 8:41–61. https://doi.org/10.1002/9781444303810.ch2

Breitsprecher K, Thorkelson DJ (2009) Neogene kinematic history of Nazca–Antarctic–phoenix slab windows beneath Patagonia and the Antarctic peninsula. Tectonophysics 464(1-4):10–20. https://doi.org/10.1016/j.tecto.2008.02.013

Breuer S, Kilian R, Weinrebe W, Schörner D, Behrmann J (2013) Glacial and tectonic control on fjord morphology and sediment deposition in the Magellan region (53°S). Mar Geol 346:31–46. https://doi.org/10.1016/j.margeo.2013.07.015

Bustos B, Folchi M, Fragkou M (2016) Coal mining on pastureland in Southern Chile; challenging recognition and participation as guarantees for environmental justice. Geoforum 84:292–304

Calderón M, Prades CF, Hervé F, Avendaño V, Fanning CM, Massonne H-J, Theye T, Simonetti A (2013) Petrological vestiges of late Jurassic-early cretaceous transition from rift to back-arc basin in southernmost Chile: new age and geochemical data from the Capitán Aracena, Carlos III and Tortuga Ophiolitic complexes. Geochem J 47:201–217

Charrier R, Pinto L, Rodríguez MP (2007) Tectonostratigraphic evolution of the Andean Orogen in Chile. In: Moreno T, Gibbons W (eds) The geology of Chile. The Geological Society, London, pp 21–114

Cifçi G, Dondurur D, Ergün M (2003) Deep and shallow structures of large pockmarks in the Turkish shelf, eastern Black Sea. Geo-Mar Lett 23(3-4):311–322. https://doi.org/10.1007/s00367-003-0138-x

Diaz-Michelena M, Kilian R (2015) Magnetic signatures of the orogenic crust of the Patagonian Andes with implication for planetary exploration. Phys Earth Planet Inter 248:35–54. https://doi.org/10.1016/j.pepi.2015.08.005

Diraison M, Cobbold PR, Gapais D, Rossello EA (1996) Tertiary kinematics of the southern Andes and the development of the Magallan Foreland Basin (Patagonia). Third ISAG, St. Malo, p 347–350

Dowdeswell JA, Vásquez M (2013) Submarine landforms in the fjords of southern Chile: implications for glacimarine processes and sedimentation in a mild glacier-influenced environment. Quat Sci Rev 64:1–19. https://doi.org/10.1016/j.quascirev.2012.12.003

Dowdeswell JA, Dowdeswell EK, Rodrigo C (2016) Pockmarks in the fjords of Chilean Patagonia. Geol Soc Lond Mem 46(1):109–110. https://doi.org/10.1144/M46.159

Duarte H, Pinheiro LM, Teixeira FC, Monteiro JH (2007) High-resolution seismic imaging of gas accumulations and seepage in the sediments of the Ría de Aveiro barrier lagoon (Portugal). Geo-Mar Lett 27(2-4):115–126. https://doi.org/10.1007/s00367-007-0069-z

Fader GBJ (1991) Gas-related sedimentary features from the eastern Canadian continental shelf. Cont Shelf Res 11(8-10):1123–1153. https://doi.org/10.1016/0278-4343(91)90094-M

Fernández R, Gulick S, Rodrigo C, Domack E, Leventer A (2017) Seismic stratigraphy and glacial cycles in the inland passages of the Magallanes region of Chile, southernmost South America. Mar Geol 386:19–31. https://doi.org/10.1016/j.margeo.2017.02.006

Geopark (2010) Geopark - Operations - Otway Block. http://www.geopark.com/homepage.htm, 11.10.2010

Glasser NF, Ghiglione MC (2009) Structural tectonic and glaciological controls on the evolution of fjord landscapes. Geomorphology 105(3-4):291–302. https://doi.org/10.1016/j.geomorph.2008.10.007

Harrington PK (1985) Formation of pockmarks by pore-water escape. Geo-Mar Lett 5(3):193–197. https://doi.org/10.1007/BF02281638

Heggland R (1998) Gas seepage as an indicator of deeper prospective reservoirs. A study based on exploration 3D seismic data. Mar Pet Geol 15(1):1–9. https://doi.org/10.1016/S0264-8172(97)00060-3

Hervé F, Pankhurst RJ, Fanning CM, Calderón M, Yaxley GM (2007) The South Patagonian batholith: 150 my of granite magmatism on a plate margin. Lithos 97(3-4):373–394. https://doi.org/10.1016/j.lithos.2007.01.007

Hidalgo E, Helle S, Alfaro G, Kelm U (2002) Geology and characterisation of the Pecket coal deposit, Magellan region, Chile. Int J Coal Geol 48(3-4):233–243. https://doi.org/10.1016/S0166-5162(01)00058-1

Hogg AG, Hua Q, Blackwell PG, Niu M, Buck CE, Guilderson TP, Heaton TJ, Palmer JG, Reimer PJ, Reimer RW, Turney CSM, Zimmermann SHR (2013) SHCAL13 southern hemispheric calibration, 0-50,000 years cal BP. Radiocarbon 55(4):1889–1903. https://doi.org/10.2458/azu_js_rc.55.16783

Hovland M, Talbot MR, Qvale H, Olaussen S, Aasberg L (1987) Methane-related carbonate cements in pockmarks of the North Sea. J Sediment Petrol 57(5):881–892

Hovland M, Gardner JV, Judd A (2002) The significance of pockmarks to understanding fluid flow processes and geohazards. Geofluids 2(2):127–136. https://doi.org/10.1046/j.1468-8123.2002.00028.x

Judd A, Hovland M (2007) Seabed fluid flow - the impact on geology, biology and the marine environment. Cambridge University Press, New York. https://doi.org/10.1017/CBO9780511535918

Kennett J, Cannariato KG, Hendy IL, Behl RJ (2003) Methane hydrates in quaternary climate change - the clathrate gun hypothesis. American Geophysical Union, Washington, D.C. https://doi.org/10.1029/054SP

Kilian R, Lamy F (2012) A review of Glacial and Holocene paleoclimate records from southernmost Patagonia (49-52°S). Quat Sci Rev 53:1–23. https://doi.org/10.1016/j.quascirev.2012.07.017

Kilian R, Hohner M, Biester H, Wallrabe-Adams HJ, Stern CR (2003) Holocene peat and lake sediment tephra record from the southernmost Chilean Andes (53-55°S). Rev Geol Chile 30(2):47–64

Kilian R, Schneider C, Koch J, Fesq-Martin M, Biester H, Casassa G, Arévalo M, Wendt G, Baeza O, Behrmann J (2007a) Palaeoecological constraints on late glacial and Holocene ice retreat in the southern Andes (53°S). Glob Planet Chang 59(1-4):49–66. https://doi.org/10.1016/j.gloplacha.2006.11.034

Kilian R, Baeza O, Steinke T, Arévalo M, Rios C, Schneider C (2007b) Late Pleistocene to Holocene marine transgression and thermohaline control on sediment transport in the western Magallanes fjord system of Chile (53°S). Quat Int 161(1):90–107. https://doi.org/10.1016/j.quaint.2006.10.043

Kilian R, Baeza O, Breuer S, Ríos F, Arz H, Lamy L, Wirtz J, Baque D, Korf P, Kremer K, Ríos C, Mutschke E, Simon M, De Pol-Holz R, Arevalo M, Wörner G, Schneider C, Casassa G (2013) Late glacial and Holocene paleogeographical and paleoecological evolution of the Seno Skyring and Otway fjord systems in the Magellanes Region. An Inst Patagonia (Chile) 41(2):7–21

King LH, MacLean B (1970) Pockmarks on the Scotian shelf. Geol Soc Am Bull 81(10):3141–3148. https://doi.org/10.1130/0016-7606(1970)81[3141:POTSS]2.0.CO;2

Kjeldsen KK, Weinrebe RW, Bendtsen J, Bjørk AA, Kjær KH (2017) Multibeam bathymetry and CTD measurements in two fjord systems in southeastern Greenland. Earth Syst Sci Data 9(2):589–600. https://doi.org/10.5194/essd-9-589-2017

Krämer K, Holler P, Herbst G, Bratek A, Ahmerkamp S, Neumann A, Bartholomä A, van Beusekom JEE, Holtappels M, Winter C (2017) Abrupt emergence of a large pockmark field in the German Bight, south-eastern North Sea. Sci Rep 7(1):5150. https://doi.org/10.1038/s41598-017-05536-1

Lamy F, Kilian R, Arz HW, Francois J-P, Kaiser J, Prange M, Steinke T (2010) Holocene changes in the position and intensity of the southern westerly wind belt. Nat Geosci 3(10):695–699. https://doi.org/10.1038/ngeo959

Maia AR, Cartwright J, Andersen E (2016) Shallow plumbing systems inferred from spatial analysis of pockmark arrays. Mar Pet Geol 77:865–881. https://doi.org/10.1016/j.marpetgeo.2016.07.029

Malkowski MA, Sharman GR, Graham SA, Fildani A (2015) Characterisation and diachronous initiation of coarse clastic

deposition in the Magallanes–Austral foreland basin, Patagonian Andes. Basin Res 2015:1–29. https://doi.org/10.1111/bre.12150

Marcon Y, Ondréas H, Sahling H, Bohrmann G, Olu K (2013) Fluid flow regimes and growth of a giant pockmark. Geology 42:63–66

Mazzini A, Svensen HH, Planke S, Forsberg CF, Tjelta TI (2016) Pockmarks and methanogenic carbonates above the giant troll gas field in the Norwegian North Sea. Mar Geol 373:26–38. https://doi.org/10.1016/j.margeo.2015.12.012

McAtamney J, Klepeis K, Mehrtens C, Thomson S, Betka P, Rojas L, Snyder S (2011) Along-strike variability of back-arc basin collapse and the initiation of sedimentation in the Magallanes foreland basin, southernmost Andes (53–54.5°S). Tectonics 30(5):TC5001. https://doi.org/10.1029/2010TC002826

Mella P (2001) Control Tectónico en la Evolución de la Cuenca de Antepaís de Magallanes, XII Región, Chile. Memoria para optar al título de Geólogo, Facultad de Ciencias Químicas, Departamento Ciencias de la Tierra, Universidad de Concepción, 149 pp

Mercer JH (1982) Holocene glacial variations in southern South America. Striae 18:35–40

Michelsen JK, Khorasani GK (1991) A regional study on coals from Svalbard: organic facies, maturity and thermal history. Bull Soc Géol France 162(2):385–397

Moernaut J, Wiemer G, Reusch A, Stark N, De Batist M, Urrutia R, Ladrón de Guevara B, Kopf A, Strasser M (2017) The influence of overpressure and focused fluid flow on subaquatic slope stability in a formerly glaciated basin: Lake Villarrica (South-Central Chile). Mar Geol 383:35–54. https://doi.org/10.1016/j.margeo.2016.11.012

Naudts L, Greinert J, Artemov Y, Beaubien SE, Borowski C, De Batist M (2008) Anomalous sea-floor backscatter patterns in methane venting areas, Dnepr paleo-delta, NW Black Sea. Mar Geol 251(3-4):253–267. https://doi.org/10.1016/j.margeo.2008.03.002

Ondréas H, Olu K, Fouquet Y, Charlou JL, Gay A, Dennielou B, Donval JP, Fifis A, Nadalig T, Cochonat P, Cauquil E, Bourillet JF, Le Moigne M, Sibuet M (2005) ROV study of a giant pockmark on the Gabon continental margin. Geo-Mar Lett 25(5):281–292. https://doi.org/10.1007/s00367-005-0213-6

Paull CK, Ussler W III, Holbrook WS, Hill TM, Keaten R, Mienert J, Haflidason H, Johnson JE, Winters WJ, Lorenson TD (2008) Origin of pockmarks and chimney structures on the flanks of Storegga slide, offshore Norway. Geo-Mar Lett 28(1):43–51. https://doi.org/10.1007/s00367-007-0088-9

Perdue EM, Koprivnjak J-F (2007) Using the C/N ratio to estimate terrigenous inputs of organic matter to aquatic environments. Estuar Coast Shelf Sci 73(1-2):65–72. https://doi.org/10.1016/j.ecss.2006.12.021

Pickrill RA (1993) Shallow seismic stratigraphy and pockmarks of a hydrothermally influenced lake, lake Rotoiti, New Zealand. Sedimentology 40(5):813–828. https://doi.org/10.1111/j.1365-3091.1993.tb01363.x

Poblete FA (2015) Formación del Oroclino Patagónico y evolución paleogeog ráfica del sistema Patagonia-Península Antártica. Doctoral Thesis at the University of Chile, Santiago, 299 p. http://repositorio.uchile.cl/handle/2250/136319

Portnov A, Vadakkepuliyambatta S, Mienert J, Hubbard A (2016) Ice-sheet-driven methane storage and release in the Arctic. Nat Commun 7:10314. https://doi.org/10.1038/ncomms10314

Ramos VA (1989) Andean foothills structures in the northern Magallanes Basin, Argentina. Am Assoc Petr Geol 73(7):887–903

Riboulot V, Cattaneo A, Sultan N, Garziglia S, Kera S, Imbert P, Voisset M (2013) Sea level change and free gas occurrence influencing a submarine landslide and pockmark formation and distribution in deep water Nigeria. Earth Planet Sci Lett 375:78–91. https://doi.org/10.1016/j.epsl.2013.05.013

Ríos F, Kilian R, Mutschke E (2016) Chlorophyll-a thin layers in the Magellan fjord system: the role of the water column stratification. Cont Shelf Res 124:1–12. https://doi.org/10.1016/j.csr.2016.04.011

Rise L, Bellec VK, Chand S, Bøe R (2015) Pockmarks in the southwestern Barents Sea and Finnmark fjords. Nor J Geol 94:263–282

Rothwell RG, Rack FR (2006) New techniques in sediment core analysis. Geol Soc Lond Spec Publ 267(1):1–29. https://doi.org/10.1144/GSL.SP.2006.267.01.01

Roy S, Hovland M, Noormets R, Olaussen S (2015) Seepage in Isfjorden and its tributary fjords, West Spitsbergen. Mar Geol 363:146–159. https://doi.org/10.1016/j.margeo.2015.02.003

Schwartz TM, Graham SA (2015) Stratigraphic architecture of a tide-influenced shelf-edge delta, upper cretaceous Dorotea formation, Magallanes-Austral Basin, Patagonia. Sedimentology 62(4):1039–1077. https://doi.org/10.1111/sed.12176

Scott AR (2002) Hydrogeological features affecting gas content distribution in coal beds. Int J Coal Geol 50(1-4):363–387. https://doi.org/10.1016/S0166-5162(02)00135-0

Sernageomin (2003) Mapa geologico de Chile version digital, escala 1: 1.000.000. Publicación Geológica Digital nr 4, CD-ROM, version 1.0, Santiago de Chile

Stern CR (2008) Holocene tephrochronology record of large explosive eruptions in the southernmost Patagonian Andes. Bull Volcanol 70(4):435–454. https://doi.org/10.1007/s00445-007-0148-z

Stern CR, Kilian R (1996) Role of the subducted slab, mantle wedge and continental crust in the generation of adakites from the Andean Austral Volcanic Zone. Contrib Mineral Petrol 123(3):263–281. https://doi.org/10.1007/s004100050155

Urien CM, Zambrano JJ, Yrigoyen MR (1995) Petroleum basins of southern South America: an overview. In: Tankard AJ, Suárez Soruco R, Welsink HJ (eds) Petroleum basins of South America, vol 62. AAPG, Memoir, Tulsa, pp 63–78

Webb K, Barnes D, Gray JS (2009) Benthic ecology of pockmarks in the inner Oslofjord, Norway. Mar Ecol Prog Ser 387:15–25. https://doi.org/10.3354/meps08079

Winsborrow M, Andreassen K, Hubbard A, Plaza-Faverola A, Gudlaugsson E, Patton H (2016) Regulation of ice stream flow through subglacial formation of gas hydrates. Nat Geosci 9(5):370–375. https://doi.org/10.1038/ngeo2696

Wölfl A-C, Wittenberg N, Feldens P, Hass HC, Betzler C, Kuhn G (2016) Submarine landforms related to glacier retreat in a shallow Antarctic fjord. Antarct Sci 28(6):475–486. https://doi.org/10.1017/S0954102016000262

Wunderlich J, Müller S (2003) High-resolution sub-bottom profiling using parametric acoustics. Int Ocean Syst 7(4):6–11